Eur. Phys. J. B **54**, 87–101 (2006)
DOI: 10.1140/epjb/e2006-00416-2

THE EUROPEAN PHYSICAL JOURNAL B

Bragg quantum wells in weak confinement regime

A. D'Andrea[a] and D. Schiumarini

Istituto dei Sistemi Complessi, CNR, via dei Taurini 19, 00185 Rome, Italy

Received 9 June 2006 / Received in final form 3 October 2006
Published online 29 November 2006 –

Abstract. The optical properties of Bragg quantum wells are studied for exciton confinement under center-of-mass quantization. A variational model of Wannier exciton envelope function, that embodies the correct boundary conditions for center-of-mass, is adopted for calculation. The present non-adiabatic exciton model is compared with adiabatic results and with heuristic "hard sphere" model. The radiative self-energy of a single-quantum well (SQW) and multi-quantum wells (MQWs) are computed in the semiclassical framework, and in effective mass approximation, by self-consistent solution of Schroedinger and Maxwell equations. This microscopic solution is free from "fitting" parameter values, except for the non-radiative broadening, and also the exciton dead-layer and the additional boundary condition are not taken ad hoc, but come coherently from the variational principle and self-consistent Schroedinger-Maxwell solution. Dispersion curves of exciton-polariton propagating in a MQW, under Bragg condition, are studied by selected numerical examples. The case of optical gap in correspondence of higher excited states is studied, and, moreover, the interesting effect of gap enhancement or inhibition, in correspondence of non-resonant Bragg energy, will be addressed.

PACS. 78.67.De Quantum wells – 71.36.+c Polaritons (including photon-phonon and photon-magnon interactions) – 71.35.Cc Intrinsic properties of excitons; optical absorption spectra – 78.67.Pt Multilayers; superlattices

1 Introduction

Recently, a new class of photonic crystals, the so called *resonant photonic crystals* (RPCs), was proposed, starting from the study of super-radiant saturation in quantum wells under Bragg condition [1–3]. In these systems, at variance of the normal photonic crystals proposed by Yablonovich [4], the dielectric function modulation is due not only to the local background dielectric function, but also to the dispersive part of non-local Wannier exciton susceptibility. Obviously, this new class of systems can not show the scalability of the optical properties, observed for normal photonic crystals. This missed property can, however, be largely compensated by "extreme" optical properties, due to the strong enhancement of the non-local dispersive part of the dielectric function for light energy close to some transition energies in the electronic gap (excitons). Therefore, this new class of systems (RPCs) are also promising for device applications.

Recently, the optical properties of Wannier excitons, strongly confined in MQWs, and under $\lambda/2$ Bragg condition, have received large attention in the literature [5–13], due to their well-known super-radiant property, while a few is published, at our knowledge, for weak confinement regime, where usually many exciton-states are present in the well [11]. The small number of papers, devoted to the optical properties of excitons under center of mass quantization, is mainly due to the difficulty of practical realization of these kind of superstructures, and moreover, from the theoretical point of view, it is also due to the scarce number of simple and reliable microscopic exciton models available in the literature [14,15].

It is well-known, that for large quantum wells the exciton center-of mass wave vector is very sensitive to the "effective volume" where the exciton is spatially confined; this volume is roughly obtained from the nominal thickness reduced by two times the "dead layer" depth [15]. While this depth value is crucially important for the optical response properties, in particular it affects the "additional boundary conditions" and the polariton self-energy, its contribution to the exciton energy becomes negligible small by increasing the quantum well thickness. Moreover, since Wannier exciton is a composite boson, the exciton mass ratio strongly influence its dynamics [14]; in particular, it shows two interesting limits, namely: (i) for $\mu/M \approx 0.25$ ($m_h \approx m_e$) the so called "positronium" limit; and (ii) for $\mu/M \to 0$ ($m_h \gg m_e$) that is the "hydrogenic" limit, where μ and M are reduced and total exciton mass respectively.

Recently, an "exact" solution for exciton confined in a large quantum well, under adiabatic approximation, was

[a] e-mail: andrea.dandrea@isc.cnr.it

proposed by Combescot et al. in reference [14]. The possibility that Wannier exciton can undergo non-adiabatic behaviour also in rather large confined systems, has given a long lasting debate in the literature [14–16], and, in our opinion, it is still an open problem.

In the present calculation we adopt a simple non-adiabatic microscopic model of Wannier envelope function under weak confinement regime given in reference [15]. This non-adiabatic exciton model embodies all the relevant physical properties present in a quantum well, namely: many exciton states due to the center-of mass quantization, and intrinsic dead-layer at well-barrier interfaces.

The aim of the present work is to discuss the fundamental properties of the optical response of Wannier exciton under center-of-mass quantization in a Bragg superlattice, coming from a microscopic self-consistent theory. Therefore, it can be divided in two parts, namely the study: (i) of the exciton properties under weak confinement regime by variational solution of the Wannier exciton model; and (ii) of the optical properties and the polariton dispersion curves for MQWs under Bragg condition.

In the present calculation, while exciton states are given in the effective mass approximation by variational minimization, the radiative self-energy in multi-quantum wells will be computed in the semiclassical framework by self-consistent solution of Schroedinger and Maxwell equations. It is well-known that the present microscopic solution is free from fitting parameters (except for the non-radiative broadening value), and also the presence of an intrinsic dead-layer in the exciton envelope function, and the propagation of additional waves in the spatial dispersive medium (that usually requires the so called "additional boundary conditions") are not introduced ad hoc, but come from the variational principle and the self-consistent Schroedinger-Maxwell solution.

The optical gap, in correspondence of higher exciton states, and the case of Bragg periodicity, out of resonance with respect to exciton states, will be addressed by selected numerical examples. Finally, the interesting property of photonic gap inhibition, induced by the competition between photonic gap and polaritonic splitting, underlines the new possibility for the gap tailoring shown by this class of resonant photonic crystals.

In Section 2, the variational exciton envelope function of reference [15], well suited for describing a Wannier exciton under weak quantum confinement regime, is revisited. The sound agreement of the former model with heuristic "hard sphere model", and with adiabatic solution [14] is pointed out in Section 3. In Section 4 the optical response of a single-quantum well and the dispersion curves of a multi-quantum wells under Bragg condition are derived analytically by a semiclassical self-consistent model in the effective mass approximation. In Section 5 the Bragg system is studied by selected numerical examples, and the interesting topic of gap tailoring in 1D resonant photonic crystal is addressed. The main results of the work are summarized in Section 6.

2 Non-adiabatic Wannier exciton in a slab: a variational solution revisited

Now we derive the non-adiabatic model of reference [15], where a Wannier exciton is confined in a slab with thickness value L many times the 3D Bohr radius ($L = \alpha\ a_B$ and $\alpha > 10$), in order to clarify the approximations involved.

Let us start by considering a Wannier exciton travelling in a bulk ($L \to \infty$). The envelope function can be given by a simple product of relative and center-of-mass motion of the electron-hole, namely: $\Psi_{ex}(\vec{r}, \vec{R}) \to \varphi_{nml}(\vec{r})\ \phi_K(Z)\, e^{i\vec{K}_\parallel \cdot \vec{R}_\parallel}$, where $\varphi_{nml}(\vec{r})$ is the hydrogenic function of the relative motion, with coordinate $\vec{r} = \vec{r}_e - \vec{r}_h$, while the total plane-wave $e^{i(\vec{K}_\parallel \cdot \vec{R}_\parallel \pm K\, Z)}$ (for $\phi_K(Z) \to e^{\pm iKZ}$) describes the center-of-mass travelling motion components (in-plane and along Z-axis respectively), where Z is the center-of-mass coordinate.

In the above limit, the exciton energy, in cylindrical coordinates, is: $E_n = E_{gap} + \varepsilon_n + E_Z + E_\parallel$, obtained by taking the top of the valence band as zero point energy, where E_{gap} is the valence-conduction energy gap at Γ point of valence-conduction band edge, and $\varepsilon_n = -R^*/n^2$ is the relative motion energy, and $E_Z + E_\parallel$ is the energy of the center-of-mass motion, with $E_Z = \hbar^2 K^2/2M$ and $E_\parallel = \hbar^2 K_\parallel^2/2M$ respectively. Therefore, the K-values are:

$$K_n = \sqrt{\frac{2M}{\hbar^2}(E - E_n)} \tag{1}$$

where K_n is real, for $E > E_n$, and imaginary for $E < E_n$.

Now, let us consider an exciton "perfectly" confined into a well of L thickness (where Z-axis is the growth direction). The Schroedinger equation of the Wannier exciton, in the two band model and in effective mass approximations, shows the hydrogenic form:

$$\hat{H}_{ex}\ \Psi(\vec{r}, Z) = \varepsilon_{ex}\ \Psi(\vec{r}, Z) \tag{2}$$

$$\hat{H}_{ex} = -\frac{\hbar^2}{2}\frac{\partial}{\partial Z}\frac{1}{M}\frac{\partial}{\partial Z}\vec{\nabla}_Z - \frac{\hbar^2}{2}\vec{\nabla}_{\vec{r}}\frac{1}{\mu}\vec{\nabla}_{\vec{r}} - \frac{e^2}{\varepsilon_B r} \tag{3}$$

obtained by neglecting the short range electron-hole exchange contribution (this term will be added as a perturbation in a second step, if necessary), and where μ and M are the reduced and the total mass of Wannier exciton respectively, and ε_{ex} is exciton eigenvalue. The exciton envelope function must undergo to the so called "no-escape boundary conditions" [15], well suited for infinite potential confinement. Therefore, the exciton peak energy is:

$$E_{ex}(\vec{K}_\parallel) = E_{gap} + \varepsilon_{ex} + \frac{\hbar^2}{2M}K_\parallel^2. \tag{4}$$

The exciton trial envelope function can be expanded in an hydrogenic basis set [15],

$$\Psi_{\vec{K}_\parallel}(\vec{r},\vec{R}) = e^{i\vec{K}_\parallel\cdot\vec{R}_\parallel}\sum_{nml}\left[a_{nml}\,e^{iK_nZ}+b_{nml}\,e^{-iK_nZ}\right]\,\varphi_{nml}(\vec{r}), \quad (5)$$

where the origin of the Cartesian axes is taken at the centre of the well slab ($-L/2 \le Z \le L/2$).

For photon energy E, greater than the lowest energy level 1S, from equation (5) we can single out the corresponding contribution (where $nml \to n$),

$$\Psi_{\vec{K}_\parallel}(\vec{r},\vec{R}) = \left\{\left[a_1\,e^{iK_1Z}+b_1\,e^{-iK_1Z}\right]\,\varphi_1(r) + \sum_{n>1}\left[a_n\,e^{iK_nZ}+b_n\,e^{-iK_nZ}\right]\,\varphi_n(r)\right\} e^{i\vec{K}_\parallel\cdot\vec{R}_\parallel}. \quad (6)$$

Now, since the system is invariant under inversion operator: $\hat{P}\equiv\begin{cases} z\to -z \\ Z\to -Z\end{cases}$, the total envelope functions can be separated in even and odd components: $\hat{P}\,\Psi_{\vec{K}_\parallel} = \pm\,\Psi_{\vec{K}_\parallel}$, namely:

$$\Psi_{even}(\vec{r},Z) = \cos(K_1Z)\,\varphi_1(r) + \sum_{\substack{n>1\\even}} b_n\,\left[e^{P_nZ} + e^{-P_nZ}\right]\,\varphi_n(r) + \sum_{\substack{n>1\\odd}} b_n\left[e^{-P_nZ} - e^{P_nZ}\right]\,\varphi_n(r)$$

$$\Psi_{odd}(\vec{r},Z) = \sin(K_1Z)\,\varphi_1(r) + \sum_{\substack{n>1\\even}} b_n\,\left[e^{-P_nZ} - e^{P_nZ}\right]\,\varphi_n(r) + \sum_{\substack{n>1\\odd}} b_n\left[e^{P_nZ} + e^{-P_nZ}\right]\,\varphi_n(r)$$

where, $K_1 = \sqrt{\frac{2M}{\hbar^2}(E - E_{gap} - \varepsilon_1 - E_\parallel)}$ and $P_n = iK_n = \sqrt{\frac{2M}{\hbar^2}(E_{gap} + \varepsilon_n + E_\parallel - E)}$ for $n > 1$.

Finally, even and odd envelope function components can be rewritten in a compact form:

$$\Psi_{even}(\vec{r},Z) = \cos(K_1Z)\,\varphi_1(r) + 2\sum_{\substack{n>1\\even}} b_n\,\cosh(P_nZ)\,\varphi_n(r) - 2\sum_{\substack{n>1\\odd}} b_n\,\sinh(P_nZ)\,\varphi_n(r) \quad (7a)$$

$$\Psi_{odd}(\vec{r},Z) = \sin(K_1Z)\,\varphi_1(r) - 2\sum_{\substack{n>1\\even}} b_n\,\sinh(P_nZ)\,\varphi_n(r) + 2\sum_{\substack{n>1\\odd}} b_n\,\cosh(P_nZ)\,\varphi_n(r). \quad (7b)$$

The analytical exciton model is based on two main approximations, namely: (i) the exciton is confined between infinite potential walls, therefore, the so called "no-escape boundary conditions" must be imposed; and (ii) all the hydrogenic virtual states are grouped in N-times degenerate average state $E_{\bar{n}}$, at the limit of the exciton continuum. The (ii) point (one-pole approximation) can be justified because the evanescent states should be very far from in energy with respect to the travelling one ($E_{\bar{n}} \to \infty$). Therefore, the quantity of equation (7a) becomes:

$$2\sum_{\substack{n>1\\even}}\cosh(P_nZ)\,b_n\;\varphi_n(r) \approx \cosh(\bar{P}_eZ)\;2\sum_{\substack{n>1\\even}} b_n\;\varphi_n(r) = \cosh(\bar{P}_eZ)\;\Phi_{ee}(\vec{r}),$$

and analogously for the other quantities of equations (7a) and (7b): $\Phi_{eo}(\vec{r})$, $\Phi_{oe}(\vec{r})$ and $\Phi_{oo}(\vec{r})$. Now, since the equations (7a) and (7b) must fulfil the no-escape boundary conditions:

$$\Psi_\alpha(z_e = \pm L/2) = \Psi_\alpha(z_h = \pm L/2) = 0 \text{ for } \alpha = \text{even, odd}, \quad (8)$$

we obtain a system of four equations that can determine the four unknowns $\Phi_{\alpha\,\beta}(\vec{r})$ (α, β = even, odd).

Finally, exciton envelope functions assume the following simple analytical form [15],

$$\Psi_{even}(\vec{r},Z) = N_e\;g_e(z,Z)\;\varphi_1(r)$$

and

$$\Psi_{odd}(\vec{r},Z) = N_o\;g_o(z,Z)\;\varphi_1(r) \quad (9a)$$

$$g_e(z,Z) = \cos(K_1Z) - \cosh(\bar{P}_e\,Z)\,F_{ee}(z) + \sinh(\bar{P}_eZ)\,F_{eo}(z)$$

$$g_o(z,Z) = \sin(K_1Z) + \sinh(\bar{P}_o\,Z)\,F_{oe}(z) - \cosh(\bar{P}_oZ)\,F_{oo}(z) \quad (9b)$$

where N_α are the normalization constants, and the inverse of evanescent coefficients $1/\bar{P}_\alpha = \delta_\alpha$ are the so called "transition layers" or "intrinsic dead-layers", while the functions $F_{\alpha\beta}(z) = \Phi_{\alpha\beta}(\vec{r})/\varphi_1(r)$, obtained by the fulfilling of the no-escape boundary conditions, are:

$$F_{ee}(z\ge 0) = \left\{\cos(K_1\,Z_1)\;\sinh\left(\bar{P}_eZ_2\right) - \cos(K_1Z_2)\;\sinh\left(\bar{P}_eZ_1\right)\right\}/\sinh\left[\bar{P}_e(Z_2 - Z_1)\right] \quad (10a)$$

$$F_{eo}(z\ge 0) = \left\{\cos(K_1\,Z_1)\;\cosh\left(\bar{P}_eZ_2\right) - \cos(K_1Z_2)\;\cosh\left(\bar{P}_eZ_1\right)\right\}/\sinh\left[\bar{P}_e(Z_2 - Z_1)\right] \quad (10b)$$

for boundary functions: $Z_1(z) = \alpha_e z - L/2$ and $Z_2(z) = -\alpha_h z + L/2$ where $0 \le z \le L$, and the electron and hole mass ratios are respectively: $\alpha_e = m_e/M$ and $\alpha_h = m_h/M$. Analogously for: $Z_1(z) = \alpha_e z + L/2$, $Z_2(z) = -\alpha_h z - L/2$ and $-L \ge z \ge 0$.

Finally, by imposing the continuity of the first derivative at $z \to 0^{\pm}$, we obtain the dispersion relationship for even wavefunctions [15]:

$$X_e \,\mathrm{tg}\,[X_e] + Y_e \,\mathrm{tgh}\,[Y_e] = 0$$

where

$$X_e = K_1 L/2,\; Y_e = \bar{P}_e L/2. \tag{11}$$

The same procedure can be adopted for computing $F_{oe}(z)$ and $F_{oo}(z)$, that for $0 \le z \le L$ are:

$$F_{oe}(z \ge 0) = \left\{\sin(K_1 Z_1)\,\cosh\left(\bar{P}_o Z_2\right) - \sin(K_1 Z_2)\,\cosh\left(\bar{P}_o Z_1\right)\right\} / \sinh\left[\bar{P}_o (Z_2 - Z_1)\right] \tag{12a}$$

$$F_{oo}(z \ge 0) = \left\{\sin(K_1 Z_1)\,\sinh\left(\bar{P}_o Z_2\right) - \sin(K_1 Z_2)\,\sinh\left(\bar{P}_o Z_1\right)\right\} / \sinh\left[\bar{P}_o (Z_2 - Z_1)\right] \tag{12b}$$

and the dispersion relationship is:

$$Y_o \,\mathrm{tg}\,[X_o] - X_o \,\mathrm{tgh}\,[Y_o] = 0$$

where

$$X_o = K_1 L/2,\; Y_o = \bar{P}_o L/2. \tag{13}$$

Notice, that the eigenvalues of center-of-mass wave vector $K_1(m)$ are $m = 1, 3, 5\ldots$ and $m = 2, 4, 6\ldots$ for even and odd envelope functions respectively [15].

Finally, an extrinsic dead-layer, as proposed by Hopfield (due to the interface disorder effect, image potential, ...), can be added in order to obtain a sound agreement with experimental spectra [16–19].

2.1 Analytical model solution

In order to compute the optical response of the system, let us consider the exciton envelope functions that show oscillator strengths different from zero (even solutions $m = 1, 3, 5, \ldots$). Notice, that odd solutions ($m = 2, 4, 6, \ldots$), for symmetry reasons, show zero oscillator strengths, but, due to the spatial dispersion effect, their polariton self-energy is different from zero; in any case they are very small with respect to the even ones. Therefore, the odd exciton states will be neglected in the present optical calculations.

The non-normalized exciton envelope function is,

$$\Psi_m(\vec{r}, Z) = g_m(z, Z)\,\varphi_1(r)$$

where $\varphi_1(r) = \exp(-r/a)/(\pi a^3)^{1/2}$ is the 1S hydrogenic wavefunction, and a is the effective Bohr radius of Wannier exciton,

$$g_m(z, Z) = \cos(K_m Z) - F_{ee}(z; K_m)\,\cosh(\bar{P}_e Z) + F_{eo}(z; K_m)\,\sinh(\bar{P}_e Z) \tag{14}$$

is the confinement function that couples relative and center-of-mass motion of the exciton, and K_m is the eigenvalue of the 1S center-of-mass wave vector (for $m = 1, 3, 5, \ldots$).

The variational parameter values are obtained by minimizing the first momentum of the Hamiltonian for the lowest exciton energy ($m = 1$) with respect to the effective Bohr radius (a), and the inverse of the transition layer ($\bar{P}_e = P = 1/\delta$) respectively,

$$\frac{\langle\Psi_1|\,\hat{H}_{ex}\,|\Psi_1\rangle}{\langle\Psi_1|\,|\Psi_1\rangle} = \min. \tag{15}$$

Finally, the inverse of the square normalization constant and the first momentum of exciton Hamiltonian, in cylindrical coordinates, are given respectively:

$$\langle\Psi_1|\,|\Psi_1\rangle = 4\pi \int_0^L dz \int_0^\infty \rho d\rho\; \varphi_1^2\left(\sqrt{\rho^2 + z^2}\right) \int_{Z_1(z)}^{Z_2(z)} dZ\; g_1^2(z, Z)$$

$$= 4\pi \int_0^L A(z)\, G_0(z)\, I_0(z)\, dz \tag{16a}$$

$$\langle\Psi_1|\,\hat{H}\,|\Psi_1\rangle = E(a)\;\langle\Psi_1|\,|\Psi_1\rangle + 4\pi \int_0^L \left\{\left[\frac{\hbar^2}{\mu a} - \frac{e^2}{\varepsilon_B}\right] G_0(z) - \frac{\hbar^2}{2M} A(z) G_1(z) - \frac{\hbar^2}{2\mu}\left[A(z) G_2(z) + 2B(z) G_3(z)\right]\right\} I_0(z)\, dz \tag{16b}$$

where $E(a)$ is the energy of the relative motion of the 1S propagating exciton, the first term in curly bracket is its correction (due to the quantum confinement), the second term is the kinetic energy of center-of-mass, and the latter term is the non-adiabatic contribution to the exciton energy. Notice, that while the functions $G_i(z)$ with $i = 0, 1, 2, 3$ are due to the confinement function of equation (14), the function $A(z)$, $B(z)$ and $I_o(z)$ come from the in plane integration of the exponential function: $\exp(-2r/a)$.

Finally, all the quantities necessary for computing energy minimization, are

$$E(a) = -\frac{\hbar^2}{2\mu}\frac{1}{a^2};\quad I_0(z) = \frac{1}{2\pi a^2}\, e^{-2|z|/a};$$
$$A(z) = |z| + a/2;\quad B(z) = -z/a, \tag{17}$$

$$G_0(z) = \int_{Z_1(z)}^{Z_2(z)} \left(g_1(z, Z)\right)^2\, dZ;$$

$$G_1(z) = \int_{Z_1(z)}^{Z_2(z)} g_1(z, Z)\, \frac{\partial^2 g_1(z, Z)}{\partial Z^2} dZ; \tag{18}$$

$$G_2(z) = \int_{Z_1(z)}^{Z_2(z)} g_1(z, Z)\, \frac{\partial^2 g_1(z, Z)}{\partial z^2} dZ;$$

$$G_3(z) = \int_{Z_1(z)}^{Z_2(z)} g_1(z, Z)\, \frac{\partial g_1(z, Z)}{\partial z} dZ$$

given in Appendix A. The former quantities are written down in a more explicit analytical form than those reported in reference [15], in order to strongly improve the numerical accuracy of computation.

It is well-known, that exciton wave vector, for well thickness many times the Bohr exciton radius, can be given by the heuristic equation of the center-of mass quantization, namely:

$$K_1(m) = m\pi/(L - 2\delta) \quad \text{where} \quad m = 1, 2, 3, \ldots, \quad (19)$$

with exciton energy: $E_m = E_{gap} - R^* + \frac{\hbar^2}{2M} K_1^2(m) + \frac{\hbar^2}{2M} K_\parallel^2$, where R^* is the exciton Rydberg value.

Now, performing the energy minimization in a rather large quantum well ($L = 16\,a$, $\varepsilon_B = 9.98$, $\mu/M = 0.063 < 0.25$), we obtain the intrinsic dead-layer value as large as two Bohr radii ($\delta = 57.0$ nm, for an effective Bohr radius $a = 28.435$ nm). Notice that the corresponding center-of-mass wave vector value of equation (11), is a bit different from the heuristic result of equation (19) (in fact we obtain $K_1 = 4.691 \times 10^{-4}$ a.u. and $K_1 = 4.805 \times 10^{-4}$ a.u. respectively). Indeed, by neglecting in equation (16b) the non-adiabatic contribution, the intrinsic dead-layer depth is strongly reduced to one Bohr radius ($\delta = 30.5$ nm), while the exciton energy is barely unchanged (a few of tenths of μeV of variation). In this limit, the center-of mass wave vector, computed by equation (11), becomes in rather sound agreement with the former heuristic result of equation (19) ($K_1 = 4.155 \times 10^{-4}$ a.u., and $K_1 = 4.166 \times 10^{-4}$ a.u. respectively).

In conclusion, while the intrinsic dead-layer depth is very sensitive to the exciton quantization, also for rather large quantum wells, the exciton energy is vanishingly affected by the dead-layer value. Indeed, the heuristic "hard sphere exciton" model of equation (19) can be easily recovered by the analytical model adopted in the present calculation.

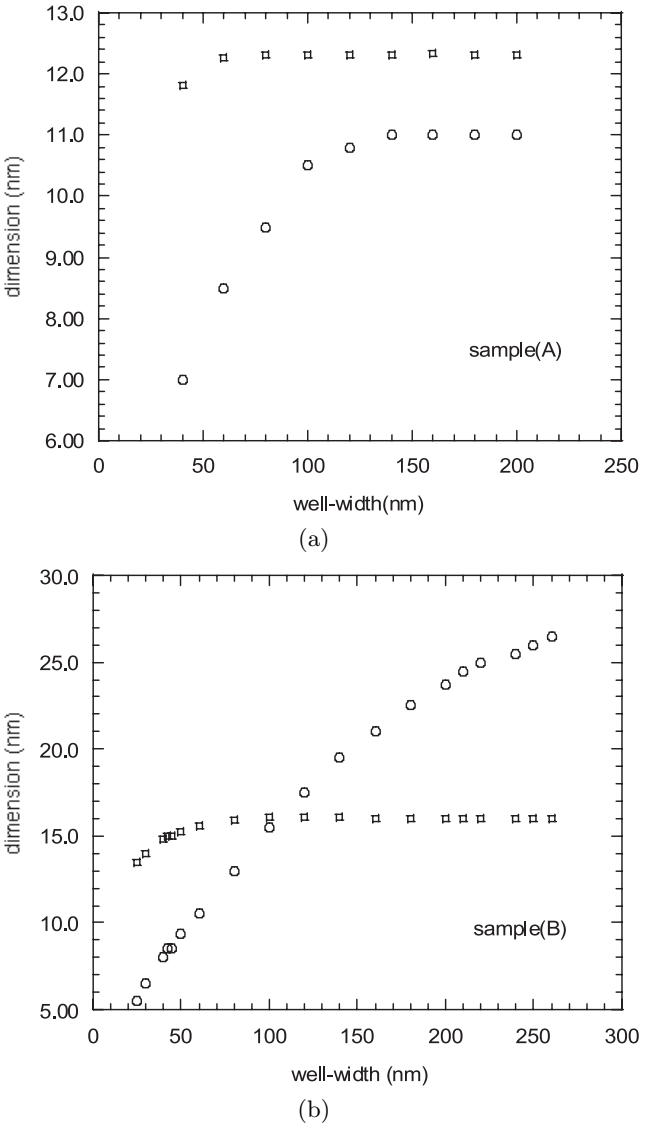

Fig. 1. Exciton variational parameters as a function of well thickness. Sample (A) and (B) are reported in Figures 2a and 2b respectively. Effective Bohr radius (a) and transition layer depth (δ) are shown by open squares and open circles respectively.

3 Wannier exciton under weak confinement

The variational computation is performed by a numerical one-dimension integration on the relative coordinate along the Z-axis quantization (see Appendix A). The parameter values adopted for the computation are:

$$\begin{aligned} & m_e = 0.077\ m_o; \quad m_h = 0.160\ m_o; \\ \text{Sample(A)} : & \mu/M = 0.22; \quad \varepsilon_B = 12.1; \\ & a_B = 12.332 \text{ nm}; \quad \text{Ryd} = -4.830 \text{ meV} \end{aligned}$$

$$\begin{aligned} & m_e = 0.038\ m_o; \quad m_h = 0.262\ m_o; \\ \text{Sample(B)} : & \mu/M = 0.11; \quad \varepsilon_B = 9.98; \\ & a_B = 15.914 \text{ nm}; \quad \text{Ryd} = -4.533 \text{ meV} \end{aligned}$$

rather close to InP (A) and GaAs (B) semiconductors, respectively.

The dead layer and exciton effective radius values, as a function of well thickness, are given in Figures 1a and 1b for sample (A) and (B) respectively. Notice, that for physical parameter values chosen, the mass ratio of sample (A) is closer to the positronium limit ($\mu/M = 0.25$) than that of sample (B). Therefore, for very large quantum wells the dead-layer of sample (A) is of the order of bulk exciton radius, while the dead-layer of sample (B) is about two times greater than that of sample (A). We would like to underline that these results, obtained for sample (A), are similar to those discussed in reference [15], while the results of sample (B), concerning rather large intrinsic dead-layer depth, have not been reported before. Moreover, the present results are also in agreement with the naïve "hard sphere exciton" model. In fact, in the classical model the positronium atom can be represented as an e–h rotating around the center-of-mass of the system, that

is located in the middle between the e–h couple; therefore the dead-layer, coming from the no-escape boundary conditions of equation (9), is about one Bohr radius, while, for the "planetary" motion of an hydrogenic atom, the dead-layer becomes two times the Bohr radius.

The exciton eigenvalues of the lowest energy state ($m = 1$), as a function of well thickness, are shown in Figures 2a and 2b for sample (A) and (B) respectively. Notice, that the zero of the exciton eigenenergies is taken at the bottom of the conduction band [15]. Sample (B) shows a faster convergence to the 2D limit than sample (A), and also this effect is due to the different energy partition between relative and center-of-mass motion of the two systems. In fact, in the hydrogenic limit, the exciton kinetic energy is essentially embodied into the relative motion, while in the positronium limit, relative and center-of-mass motion are both effective, till to the 2D value, where the center-of mass motion is completely quenched. In the insets of Figure 2, the even $m = 1, 3, 5, 7$ exciton states are also shown for a large range of energies. These rather unphysical energies come from the infinite walls model adopted for quantum exciton confinement where no upper energy limit is embodied (except for the evanescent state that will be in energy far from the propagating one). In order to obtain sensible results for higher exciton energy states a more refined propagating envelope function is necessary, where also the second ($n = 2$) hydrogenic functions become propagating. This more refined model can be obtained by substitution: $\varphi_{1S}(\vec{r}) \rightarrow \varphi_{1S}(\vec{r}) + \alpha\,\varphi_{2S}(\vec{r}) + \beta\,\varphi_{2P}(\vec{r})$ in equations (7a) and (7b), with α and β variational parameters [20].

In Figure 3 the exciton dead-layer as a function of the mass ratio μ/M in the Bohr radius unit is shown. The results, obtained with the present non-adiabatic variational model, are compared with the adiabatic ones of reference [14]. The agreement between the two different models is sound, and the qualitative interpretation, based on the naïve hard sphere exciton model, is confirmed for both the models [21]. In conclusion, the present analytical model shows the correct behaviour of Wannier exciton under center-of-mass quantization, while no-contradiction with the results of reference [14] or with the hard sphere model comes from the variational minimization [21].

Finally, we would like to underline that the present results give also an interesting contribution to the long lasting debate about adiabatic and non-adiabatic solutions for exciton quantization in large quantum wells (see Ref. [16] pp. 392–397 and 413–414).

4 Optical response in single and multi-quantum wells

Let us consider a Wannier exciton confined in a single quantum well of sample (B), with thickness L, and clad between two infinite barriers. The even exciton envelope function is:

$$\Psi_m(\vec{r}, Z; \vec{K}_{\|}) = N_m\, g_m(z, Z)\, \varphi_1(r)\, e^{i\vec{K}_{\|}\cdot\vec{R}_{\|}}/\sqrt{S} \qquad (20)$$

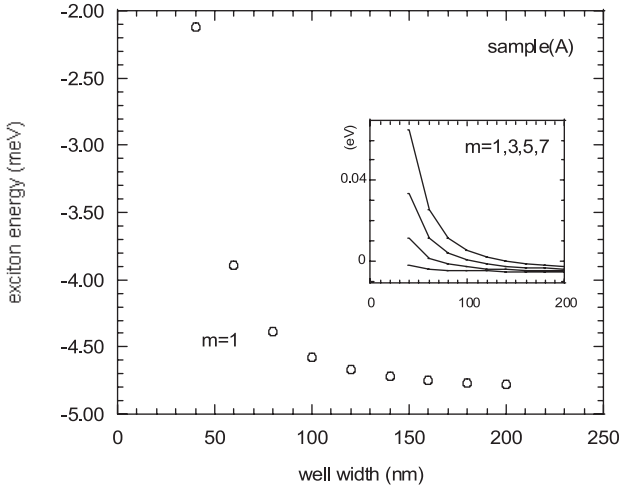

(a)

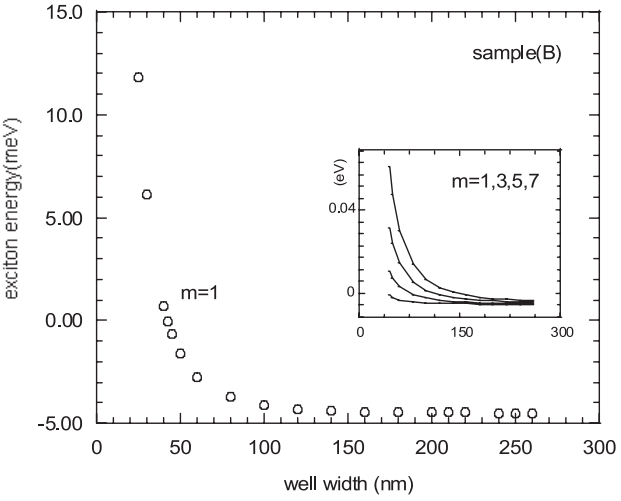

(b)

Fig. 2. Lowest exciton eigenenergy ($m = 1$) as a function of quantum well thickness for sample (A) and (B) are shown in Figures 3a and 3b respectively. The four lowest eigenenergies ($m = 1, 3, 5, 7$) are given in the insets.

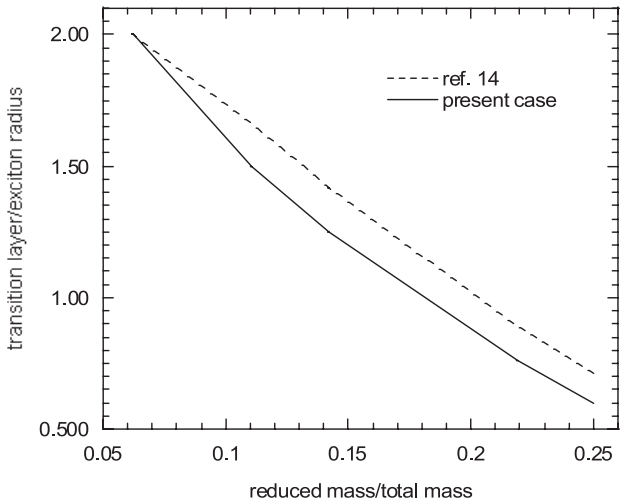

Fig. 3. The ratio δ/L as a function of masses ratio (μ/M) is shown by solid curve. The results obtained in reference [14] is also reported (dashed curve) for sake of comparison.

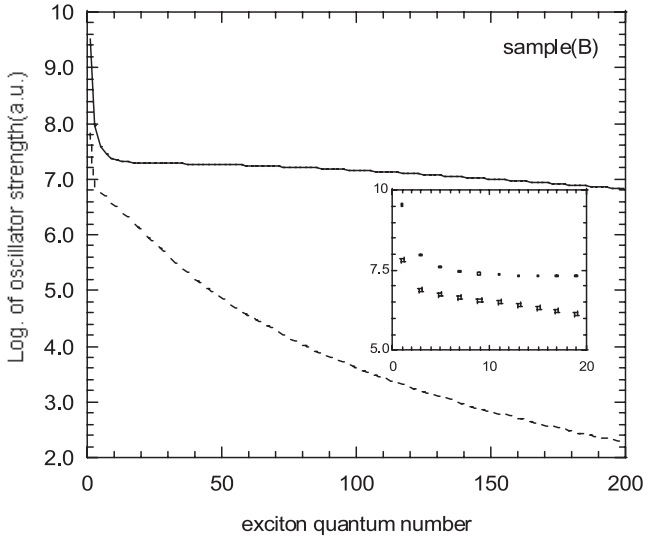

Fig. 4. Oscillator strengths of even exciton states as a function of exciton quantum number ($n = 1, 3, 5, \ldots$) for sample (B), and two well thicknesses: $L = 260$ nm (solid line) and $L = 25$ nm (dashed line). In the inset oscillator strengths for $m \leq 20$ exciton states are shown.

where N_m are the normalization constants of mth exciton state ($m = 1, 3, 5, \ldots$), and $g_m(z, Z)$ are the confinement functions given in equation (14).

The oscillator strength for even states of Wannier exciton, as a function of the center-of-mass quantum number m is,

$$f^{(m)}/S = g\frac{E_K}{\hbar\omega} \quad \left| \int_{-L/2}^{L/2} \Psi_m(\vec{r}=0, Z) dZ \right|^2 \tag{21}$$

where g is the band degeneracy, $E_K = 23$ eV is the Kane's energy, and the resonant photon energy is $\hbar\omega_o = E_{gap} + E_m$ where E_{gap} is the electron energy gap and $k_\parallel = 0$. The exciton envelope function for $\vec{r} = 0$ is:

$$\Psi_m(\vec{r}=0, Z) = \frac{N_m}{\sqrt{\pi a^3}} \left\{ \cos(K_m Z) - \cosh(PZ) \frac{\cos(K_m L/2)}{\cosh(PL/2)} \right\}. \tag{22}$$

In Figure 4 the oscillator strength for surface unit is computed for two different slab thicknesses $L = 260$ nm ($L \approx 16\,a$) and $L = 25$ nm ($L \approx 2\,a$), and for the parameter values of the sample (B).

Note that the thin slab converges to the oscillator strength of the lowest exciton state faster than the thick one. Moreover, the oscillator strength of the slab is essentially embodied in the lower exciton energy states, as it is clearly shown in the inset of Figure 4. In fact, $f^{(m)}/S$ strongly decreases for the first six even states ($m = 1, 3, 5, 7, 9, 11$); therefore, in order to take into account a rather extended exciton state basis set, these states will be embodied in the optical spectra calculation.

The non-local exciton polarization, expanded in the center-of mass basis set, is [15]:

$$\begin{aligned}\vec{P}\left(\vec{K}_\parallel, Z\right) &= \sum_m \int_0^L dZ'\, \chi_m(\vec{K}_\parallel; Z, Z')\, \vec{E}\left(\vec{K}_\parallel, Z'\right) \\ &= \sum_m \frac{S_o(\omega)}{E_m(\vec{K}_\parallel) - \hbar\omega - i\Gamma_{NR}(\omega)} \Psi_m^*\left(\vec{r}=0, Z; \vec{K}_\parallel\right) \\ &\quad \times \int_0^L dZ'\, \Psi_m\left(\vec{r}=0, Z'; \vec{K}_\parallel\right)\, \vec{E}\left(\vec{K}_\parallel, Z'\right) \end{aligned} \tag{23}$$

where $\chi_m(\vec{K}_\parallel; Z, Z')$ is the optical susceptibility for cubic crystal, $\Gamma_{NR}(\omega)$ is the non-radiative broadening, and $S_o(\omega)$ embodies the Kane's energy E_K of the interband transition, namely: $S_o(\omega) = g\frac{E_K}{\omega^2}\frac{e^2}{m_o}$. The exciton energy is:

$$E_m(\vec{K}_\parallel) = E_{gap} + E_m + \frac{\hbar^2}{2M} K_\parallel^2. \tag{24}$$

The Maxwell equation for S polarization, with X and Z Cartesian axis parallel and normal to the slab surfaces respectively ($\vec{K}_\parallel \| \hat{x}$), is:

$$\frac{\partial^2 E_y}{\partial x^2} + \frac{\partial^2 E_y}{\partial z^2} = -\frac{\omega^2}{c^2} D_y(x, z) \tag{25}$$

where,

$$E_y(x, z) = E_y(z)\, e^{ik_\parallel x}$$

and

$$\begin{aligned} D_y(x, z) &= D_y(z)\, e^{ik_\parallel x} = [\varepsilon_b E_y(z) + 4\pi P_y(z)]\, e^{ik_\parallel x}, \\ \frac{\partial^2 E_y}{\partial z^2} &+ \left[\frac{\omega^2}{c^2}\varepsilon_b - k_\parallel^2\right] E_y(z) = -4\pi\frac{\omega^2}{c^2} P_y(z), \end{aligned} \tag{26}$$

where the exciton-photon interaction (polariton) is characterized by the same in plane wave vector $\vec{K}_\parallel = k_\parallel\, \hat{i}$ values for the two particles. The former Maxwell integral-differential equation can be transformed in an integral equation by using the Green's function formalism:

$$\left\{\frac{\partial^2}{\partial z^2} + k_z^2\right\} g(z, z') = \delta(z - z') \tag{27}$$

where

$$k_z = \left[\frac{\omega^2}{c^2}\varepsilon_b - k_\parallel^2\right]^{1/2},$$

whose solution is: $g(z, z') = \frac{1}{2ik_z}\, e^{ik_z|z-z'|}$.

Finally, equation (26) can be given as a Lippmann-Schwinger integral equation:

$$E_y(z) = E_y^o(z) - 4\pi\frac{\omega^2}{c^2} \sum_m \int\int g(z, z')\, \chi_m(z', z'')\, E_y(z'') dz' dz''. \tag{28}$$

In Appendix B this integral equation in a quantum well is exactly solved.

$$\begin{pmatrix} \left[e^{iKd} - (1+\Delta_o(\omega))\, e^{ik_z d}\right] & -\Delta_{--}(\omega)\, e^{ik_z d} \\ \Delta_{++}(\omega)\, e^{iKd} & \left[(1+\Delta_o(\omega))\, e^{iKd} - e^{-ik_z d}\right] \end{pmatrix} \begin{pmatrix} A \\ B \end{pmatrix} = 0. \quad (33)$$

4.1 Generalized Kroening-Penney model

The optical dispersion curves of a MQWs can be obtained by the generalized Kroening-Penney model. Since we are interested into the optical response of the Wannier exciton, let us take constant the background dielectric function ($\varepsilon(z) = \varepsilon_b$); in this case, the optical dispersion curves show fully polaritonic character.

The electric fields in the left and right barrier of the well are given by equation (7) of Appendix B, in the two different limits:
Left

$$(Z \to 0) \quad E_y(z \le z') = A\, e^{ik_z z} + \left[A\, \Delta_{++}(\omega) + B\, (1 + \Delta_{+-}(\omega))\right]\, e^{-ik_z z} \quad (29a)$$

Right

$$(Z \to L) \quad E_y(z \ge z') = \left[A\, (1 + \Delta_{-+}(\omega)) + B\, \Delta_{--}(\omega)\right]\, e^{ik_z z} + B\, e^{-ik_z z} \quad (29b)$$

where Δ quantities, for real envelope function basis set, are given by:

$$\Delta_{\pm\mp}(\omega) = -\frac{\omega^2}{c^2}\frac{1}{2ik_z}\sum_m S_m(\omega)\, \varphi_m(\pm k_z) \times \sum_{m'}\left[\left(\overleftrightarrow{I} + \overleftrightarrow{M}(\omega)\right)^{-1}\right]_{m,m'} \varphi_{m'}(\mp k_z) \times e^{\pm ik_z L/2 \mp ik_z L/2} \quad (30)$$

and $\varphi_m(k_z) = \int_{-L/2}^{L/2} \Psi_m(\vec{r}=0, z)\, e^{ik_z z} dz$ is the Fourier transform of the exciton envelope function computed for $\vec{r} = 0$, while $S_m(\omega) = \frac{S_o(\omega)}{E_m(\vec{K}_\parallel) - \hbar\omega - i0^+}$. Notice, that $\overleftrightarrow{I}$ is the unit matrix, while all the quantities necessary for computing the $\Delta(\omega)$ quantity of equation (30), are defined and given in the explicit form in Appendix C.

The reflection and transmission coefficients for a single quantum well are given by imposing the conditions $A = 1$ and $B = 0$, therefore:

$$r_s(\omega) = \Delta_{++}(\omega) \quad \text{and} \quad t_s(\omega) = 1 + \Delta_{-+}(\omega) \quad (31a)$$

while the absorbance is:

$$A_s(\omega) = 1 - |r_s(\omega)|^2 - |t_s(\omega)|^2. \quad (31b)$$

Finally, by imposing the periodicity condition,

$$E_y^{(L)}(z)\, e^{iKd} = E_y^{(R)}(z + d) \quad (32)$$

and, noticing that $\Delta_{+-}(\omega) = \Delta_{-+}(\omega) \equiv \Delta_o(\omega)$, we obtain:

$$\left\{A\, e^{ik_z z} + \left[A\, \Delta_{++}(\omega) + B\, (1 + \Delta_o(\omega))\right]\, e^{-ik_z z}\right\}\, e^{iKz} = \left[A\, (1 + \Delta_o(\omega)) + B\, \Delta_{--}(\omega)\right]\, e^{ik_z(z+d)} + B\, e^{-ik_z(z+d)}.$$

By separating forward and backward propagation waves, the periodicity condition is given under 2×2 matrix form:

See equation (33) above.

Now, since the determinant of coefficient matrix is equal zero, an implicit equation in K and ω is obtained:

$$(1 + \Delta_o(\omega))\, e^{2iKd} - \left\{\left[(1 + \Delta_o(\omega))^2 - \Delta_{++}(\omega)\Delta_{--}(\omega)\right] \times e^{ik_z d} + e^{-ik_z d}\right\}\, e^{iKd} + (1 + \Delta_o(\omega)) = 0$$

that can be simplified:

$$\cos(Kd) = \frac{1}{2}\left\{\left[(1 + \Delta_o(\omega)) - \frac{\Delta_{++}(\omega)\Delta_{--}(\omega)}{1 + \Delta_o(\omega)}\right] e^{ik_z d} + e^{-ik_z d}\right\} \equiv f(\omega) \quad (34)$$

and finally, the polariton dispersion curves in explicit form is: $Kd = \arccos[f(\omega)]$.

5 Optical properties of exciton in weak confinement: numerical results

Let us consider a single quantum well of thickness about two Bohr radii ($L \approx 2\ a_B$). It is well-known, that for this thickness value the Wannier exciton is close to the so called $2D \to 3D$ transition [15–17], where the exciton behaviour is very sensitive to slab thickness value, while, the exciton levels become strongly separated in energy.

The variational parameter values, adopted for the calculation, are those of sample (B) for a well thickness $L = 25$ nm, namely: $a = 13.45$ nm the exciton effective Bohr radius, and $\delta = 5.5$ nm the exciton transition layer depth. The mass ratio is $\mu/M = 0.11062$, that is an intermediate value between hydrogenic ($\mu/M \to 0$) and positronium ($\mu/M = 0.25$) limits. In this case, the two lowest exciton states ($m = 1, 3$) have energy values: $E_1 = E_{gap} + \varepsilon_{m=1} = 1.5118$ eV and $E_3 = 1.5445$ eV, where $E_{gap} = 1.5$ eV (close to the GaAs energy gap at $T = 2$ K°), while the oscillator strength ratio, between the first and the second even exciton states, is: $f^{(3)}/f^{(1)} = 1/10$ (see the inset of Fig. 4).

It is well-known, that the self-consistent solution of the Maxwell equation gives the correct self-energy of the radiation-matter interaction, and a non-radiation broadening only should be added to the non-local dielectric

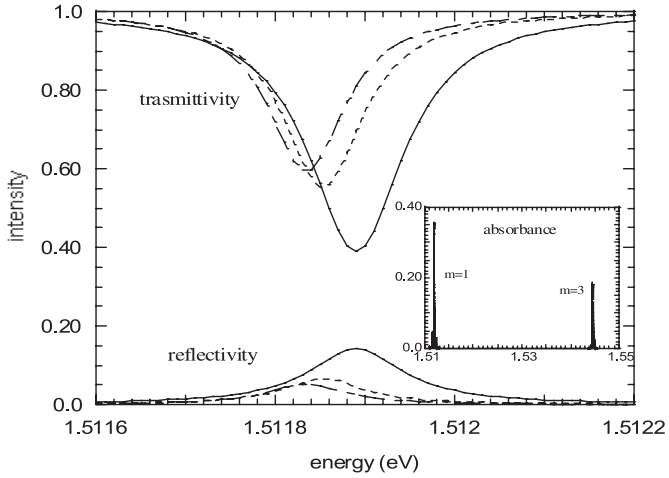

Fig. 5. Reflection and transmission spectra for the lowest exciton states ($m = 1$) of sample (b) computed for three different values of incidence angle, namely: 0° 30° 60°. Absorbance spectrum at normal incidence for $m = 1, 3$ exciton states is shown in the inset.

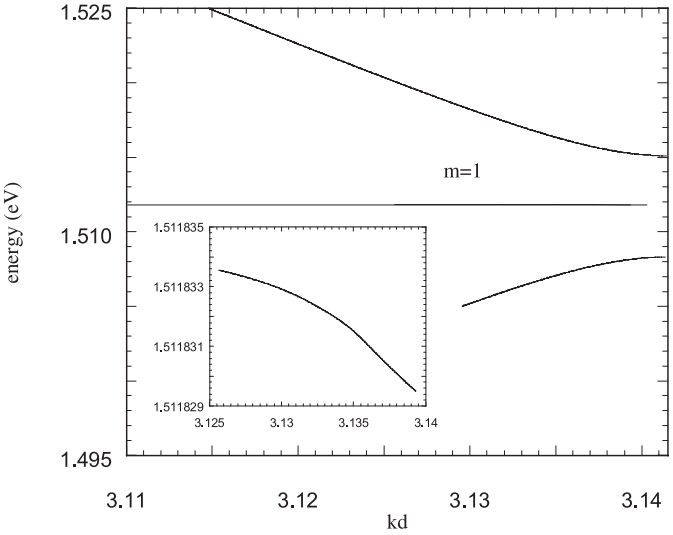

Fig. 6. Photonic energy gap, in resonance with the lowest exciton state $m = 1$, is shown. The radiative energy can be observed in the inset, where an enlarged energy scale is used for the central dispersion curve.

function (see Eq. (23)). In the present calculation the broadening is taken constant and rather small ($\Gamma_{NR} = 40\ \mu$eV), roughly of the same order of magnitude of the radiation broadening (about 15 μeV).

The optical spectra for S polarization, computed in the range of the lowest exciton energy state ($m = 1$), are shown in Figure 5 for three different angles of incidence, namely: $\theta = 0°$, 30° and 60° degrees. The reflectivity increases by increasing the incident angle value, while an opposite behaviour is shown for the transmittivity. The absorbance spectrum, computed for energy range close to the first and the third exciton states at normal incidence, is shown in the inset of Figure 5. The intensity ratio scales as the corresponding oscillator strength values.

Since the optical response shows the correct behaviour as a function of the incidence angle of the light, we can be confident that also the dispersion curves of MQWs under Bragg condition, that will be discussed in the next section, should describe the correct physical behaviour of the exciton-polariton.

5.1 Polariton dispersion in MQWs Bragg reflector

A multi-quantum wells under Bragg conditions is a prototype of $1D$ resonant photonic crystals for quantum well number $N \to \infty$. Recently, Cho (Ref. [2]) has pointed out that the optical response for very thin quantum wells undergoes a transition from super-radiant regime to the $1D$ polariton gap as a function of quantum well number N. This interesting phenomenon was revisited, two years later, by Cho and one of the present author (see Ref. [3]).

Now, in the present work we have extended the study of $1D$ resonant photonic crystal ($N \to \infty$) to the case of thick quantum wells, where, due to the center-of mass quantization, rather dense exciton states can appear in the optical spectrum of the system, and competition between polariton splittings and optical gap can give the interesting phenomenon of the gap enhancement or inhibition.

Let us consider a quantum well with the same parameter values given in the former section where the center-of-mass exciton levels are well separated in energy. The polariton dispersion curves are computed by equation (34), along $\Gamma \to Z$ direction ($\vec{K}_{\|} = 0$), and by taking the non-radiation broadening value: $\Gamma_{NR} = 0$.

When the former quantum well is embodied in a Bragg's reflector with the periodicity $d_1 = \lambda_1/2 = 129.763$ nm, computed for light energy in resonance with the $m = 1$ exciton level, it is well-known [1–3] that the periodicity reduces the straight line of the light dispersion in a segmented line (confined into the first Brillouin zone), while the exciton-photon interaction opens the optical gap in the correspondence of the $m = 1$ exciton energy. In fact, for photon energies close to the lowest exciton energy, the characteristic three branches dispersion curves [1,3] are shown in Figure 6.

The central dispersion curve is in coincidence with the $m = 1$ exciton-polariton energy, and its behaviour is reported in an expanded energy scale in the inset, where the radiative self-energy value can be evaluated (15 μeV). Notice, that this value is in sound agreement with optical response results obtained for a SQW [1–3].

The present result is completely analogous to that obtained for thin quantum wells (see Refs. [3,4]), while many polariton splittings open in correspondence with higher energy exciton states ($m > 1$) [11].

In Table 1 the optical gap for $m = 1$ and the polariton splitting at higher energy states ($m > 1$) are given.

Now, we can move the optical gap at higher energy by taking the Bragg periodicity in resonance with $m = 3$

Table 1. Polariton splitting energies for even exciton states ($m = 1, 3, 5, 7, 9, 11$), and for Bragg condition in resonance with $m = 1$ exciton state.

	$m = 1$ gap	$m = 3$	$m = 5$	$m = 7$	$m = 9$	$m = 11$
ΔE(meV)	6.769	0.132	0.037	0.018	0.011	0.006

Table 2. Polariton splitting energies for even exciton states, and for Bragg condition in resonance with $m = 3$ exciton state.

	$m = 1$	$m = 3$ gap	$m = 5$	$m = 7$	$m = 9$	$m = 11$
ΔE(meV)	0.357	4.209	0.058	0.022	0.012	0.007

exciton level, namely: $d_3 = \lambda_3/2 = 127.017$ nm. The dispersion curves, computed for a large range of light energy are shown in Figure 7a, while in Figure 7b the characteristic three branches dispersion curves, close to the photonic gap, and the polaritonic splittings for $m = 1, 5$ exciton states are reported in an enlarged energy scale.

The energy gap for $m = 3$ is about 4.21 meV, that is lower than that observed for $m = 1$, and also the radiation self-energy values, not reported here, are smaller than the present ones. Polariton splittings, and energy gap are given in more detail in Table 2.

Notice, that the higher energy polariton splittings are systematically higher than those computed before (see Tab. 1), while for higher m-value the convergence at the same polariton splitting is reached rather slowly. Moreover, it is interesting to notice that, while the oscillator strength ratio between the two levels is 1/10, as shown before for a SQW (see the inset of Fig. 4), the ratio between their radiation broadenings is now greater than 10/1 due to the Bragg effect in resonance with $m = 3$ exciton state.

The optical results shown before are obtained for a quantum well thickness as large as two Bohr radii, therefore in the zone of the $3D - 2D$ transition of Wannier exciton, very close to the quantum well limit. Now, let us consider a Wannier exciton under center-of-mass quantization with quantum well thickness many times the Bohr radius. It is well known that for rather large quantum wells, exciton levels can become closer in energy than the non-radiative broadening value, and, therefore, their optical spectrum, due to a convolution of many exciton states, can appear as an asymmetric exciton peak, with a long tail towards the high energy side of the spectrum [18,19]. In this limit, there is no point by taking the Bragg periodicity in resonance with a particular exciton level, but it is sufficient to choose the periodicity in the energy range of the convolution. For MQWs close to this condition, strong distortion in the polaritonic dispersion curves is expected, due to the competition between optical gap and polariton splitting effects.

In fact, let us take as parameter values of the single well: $L = 5$ $a = 80$ nm, $a = 16$ nm, $\delta = 13$ nm, and Bragg periodicity of about $d = 130.9721$ nm, that shows light energy resonance at $\hbar\omega_o = 1.4979$ eV that drops between $m = 1$ and $m = 3$ exciton levels. In this case, by

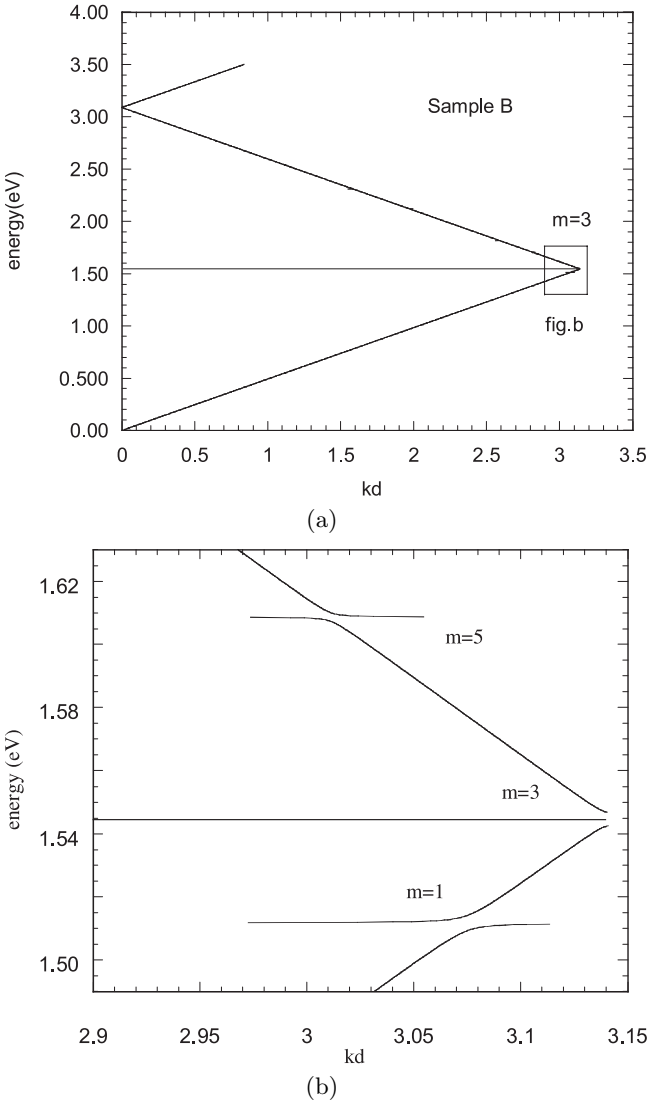

Fig. 7. Polariton dispersion curves of a quantum well Bragg superlattice for resonant light energy in coincidence with the $m = 3$ exciton state are shown in (a). Photonic energy gap, in resonance with $m = 3$ exciton state, and polariton splittings for $m = 1, 5$ are shown in an enlarged energy scale in (b).

performing calculation for the lowest energy exciton state ($m = 1$) the dispersion curves show three branches (with energy gap $E_{gap} = 2.7$ meV) as reported in Figure 8. This dispersion curves look very similar to those discussed before (Figs. 6 and 7b), and only a small distortion in the central branch appears. Indeed, by comparing this upward distortion with downward one, shown in the inset of Figure 6, we can derive the sign of the detuning between exciton and Bragg energy of the system simply analyzing the different dispersion behaviours (up or down) of the central polariton curve.

Let us perform calculation by taking into account the six lowest exciton states (m =1–11) of the quantum well. The results are shown in Figure 9 in the range of resonant photon energy; in this case at variance of the usual

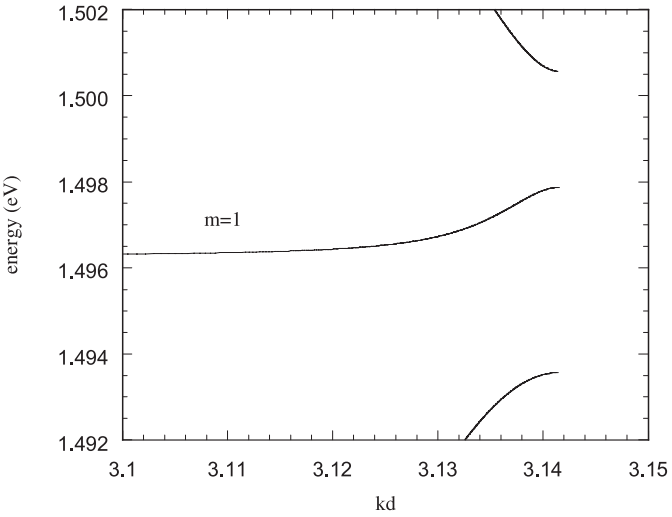

Fig. 8. Dispersion curves of a quantum well Bragg superlattice computed for rather thick quantum well $L = 5\ a$, for periodicity out of resonance with respect of the exciton states. The computation take into account the lowest exciton state ($m = 1$) only.

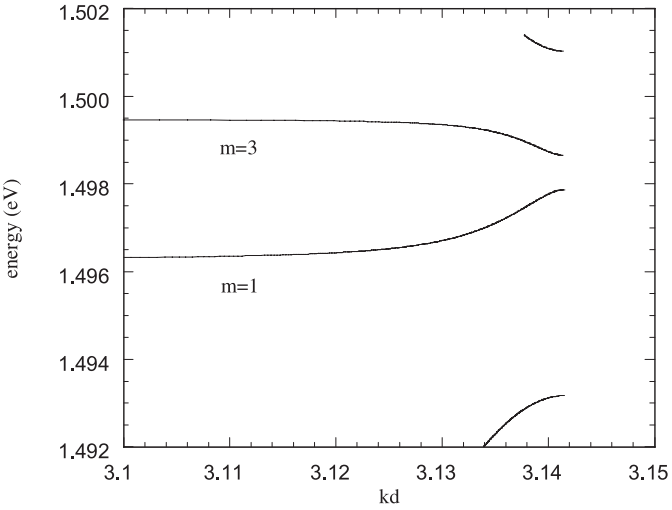

Fig. 9. Dispersion curves of a quantum well Bragg superlattice computed for rather thick quantum well $L = 5\ a$, for periodicity out of resonance with respect to the exciton states. The computation take into account the lowest six energy exciton states (m =1–11).

three dispersion curves a more complicated pattern of four curves is observed. While, in correspondence of $m = 1$ and $m = 3$ exciton states, normal polariton splitting values are observed (of 5.50 meV and 1.55 meV respectively), a rather small photonic gap (about 0.77 meV) appears, in the correspondence of the resonant photon energy $\hbar\omega_o$ (probably, this value is very close to the first odd exciton state $m = 2$). Therefore, the energy gap effect is strongly reduced by the synergic effect of the two polariton states located at lower and higher energy respectively.

Finally, "extreme" optical properties should be obtained also for the case of a finite number of quantum wells ($N < 80$) in the zone of the optical super-radiance effect. In this case it should be possible to obtain a huge enhancement of the radiative self-energy also for odd exciton states($m = 2, 4, 6, \dots$) [21].

6 Conclusions

In conclusion, a variational exciton envelope function, well suited for describing exciton behaviour under center-of-mass quantization, is revisited [15]. New results are obtained for the intrinsic dead layer depth, and for the spatial dispersion behaviour of Wannier exciton. A contribution to the long lasting debate, present in the literature [14–16], concerning the adiabatic and non-adiabatic approximations, is given.

Optical properties of a SQW and dispersion curves of a MQWs under $\lambda/2$ Bragg condition are computed in the semiclassical framework, and in effective mass approximation, by self-consistent solution of Schroedinger and Maxwell equations. This microscopic solution is free from "fitting" parameter values, and from ad hoc physical assumptions (dead-layer and ABCs).

In principle, the control of the periodicity in a resonant $\lambda/2$ Bragg reflector allows to perform the tailoring of the optical gap of the system by modulating the real part of the non-local dielectric function of Wannier exciton [3]. Obviously, in real systems also the modulation of the background dielectric function should be taken into account, and this contribution can enrich the possibilities of the optical tailoring of the model.

The case of the optical gap in correspondence of higher excited states is pointed out by selected numerical examples. Indeed, the inhibition of the photonic gap, induced by the competition with polariton states, underlines the new possibility in the gap tailoring shown by this class of resonant photonic crystals.

The authors are indebted with the Project FIRB-MIAO of MIUR of Italy (WP2.2-task3) for financial support, and with Dr. L. Pilozzi for the critical reading of the manuscript.

Appendix A

In order to minimize the variational energy of equations (16a) and (16b) of the text, we must to compute the following quantities:

$$G_0(z) = g_0(z) + \left[g_1(z)\, F_e^2(z) + g_2(z)\, F_o^2(z)\right] - 2\left[g_3(z)\, F_e(z) - g_4(z)\, F_o(z)\right] - 2g_5(z)F_e(z)F_o(z) \tag{A.1}$$

$$G_1(z) = -K^2 g_0(z) + P^2\left[g_1(z)\, F_e^2(z) + g_2(z)\, F_o^2(z)\right] + \left(K^2 - P^2\right)\left[g_3(z)\, F_e(z) - g_4(z)\, F_o(z)\right] - 2P^2 g_5(z)F_e(z)F_o(z); \tag{A.2}$$

$$[A(z)G_2(z)+2B(z)G_3(z)] = -P^2\,A(z)\,G_4(z) + \frac{M(z)}{\sinh\left(P(Z_2(z)-Z_1(z))\right)}\{2B(z)R_e(z)+A(z)\,[S_e(z) +2R_e(z)\coth\left(P(Z_2(z)-Z_1(z))\right)]\} + \frac{N(z)}{\sinh\left(P(Z_2(z)-Z_1(z))\right)}\{2B(z)R_o(z)+A(z)\,[S_o(z) +2R_o(z)\coth\left(P(Z_2(z)-Z_1(z))\right)]\} \quad \text{(A.3)}$$

where, the latter term, connected with the non-adiabatic contribution, is computed by the following quantities:

$$G_4(z) = \left[g_1(z)\,F_e^2(z)+g_2(z)\,F_o^2(z)\right]-[g_3(z)\,F_e(z) -g_4(z)\,F_o(z)]-2g_5(z)F_e(z)F_o(z); \quad \text{(A.4)}$$

$$\begin{aligned} S_e(z) = {} & \left(\alpha_h^2P^2-\alpha_e^2K^2\right)\sinh\left(PZ_2(z)\right)\cos\left(KZ_1(z)\right) \\ & +\left(\alpha_h^2K^2-\alpha_e^2P^2\right)\sinh\left(PZ_1(z)\right)\cos\left(KZ_2(z)\right) \\ & -2\alpha_e\alpha_hKP\left[\cosh\left(PZ_1(z)\right)\sin\left(KZ_2(z)\right)\right. \\ & \left.-\cosh\left(PZ_2(z)\right)\sin\left(KZ_1(z)\right)\right] \end{aligned}$$

$$\begin{aligned} S_o(z) = {} & \left(\alpha_h^2P^2-\alpha_e^2K^2\right)\cosh\left(PZ_2(z)\right)\cos\left(KZ_1(z)\right) \\ & +\left(\alpha_h^2K^2-\alpha_e^2P^2\right)\cosh\left(PZ_1(z)\right)\cos\left(KZ_2(z)\right) \\ & -2\alpha_e\alpha_hKP\left[\sinh\left(PZ_1(z)\right)\sin\left(KZ_2(z)\right)\right. \\ & \left.-\sinh\left(PZ_2(z)\right)\sin\left(KZ_1(z)\right)\right] \end{aligned}$$

$$\begin{aligned} R_e(z) = {} & P\cosh\left(P(Z_2(z)-Z_1(z)\right)\,F_e(z) \\ & -\left[K\left(\alpha_e\sinh\left(PZ_2(z)\right)\sin\left(KZ_1(z)\right)\right.\right. \\ & \left.\left.+\alpha_h\sinh\left(PZ_1(z)\right)\sin\left(KZ_2(z)\right)\right)\right] \\ & -\left[P\left(\alpha_e\cosh\left(PZ_1(z)\right)\cos\left(KZ_2(z)\right)\right.\right. \\ & \left.\left.+\alpha_h\cosh\left(PZ_2(z)\right)\cos\left(KZ_1(z)\right)\right)\right] \end{aligned}$$

$$\begin{aligned} R_o(z) = {} & P\cosh\left(P(Z_2(z)-Z_1(z)\right)\,F_o(z) \\ & -\left[K\left(\alpha_e\cosh\left(PZ_2(z)\right)\sin\left(KZ_1(z)\right)\right.\right. \\ & \left.\left.+\alpha_h\cosh\left(PZ_1(z)\right)\sin\left(KZ_2(z)\right)\right)\right] \\ & -\left[P\left(\alpha_e\sinh\left(PZ_1(z)\right)\cos\left(KZ_2(z)\right)\right.\right. \\ & \left.\left.+\alpha_h\sinh\left(PZ_2(z)\right)\cos\left(KZ_1(z)\right)\right)\right] \end{aligned}$$

$$M(z) = F_e(z)\,g_1(z)-g_3(z)-F_o(z)\,g_5(z);$$

$$N(z) = F_o(z)\,g_2(z)-g_4(z)-F_e(z)\,g_5(z). \quad \text{(A.5)}$$

Finally, all the former quantities are computed by the functions $g_\ell(z)$ for $\ell = 0,1,2,3,4,5$, that are given by,

$$\begin{aligned} g_0(z) &= \left[\frac{Z}{2}+\frac{1}{4K}\sin\left(2KZ\right)\right]_{Z_1(z)}^{Z_2(z)}; \\ g_1(z) &= \left[\frac{Z}{2}+\frac{1}{4K}\sinh\left(2PZ\right)\right]_{Z_1(z)}^{Z_2(z)}; \\ g_2(z) &= \left[-\frac{Z}{2}+\frac{1}{4P}\sinh\left(2PZ\right)\right]_{Z_1(z)}^{Z_2(z)}; \\ g_5(z) &= \left[\frac{1}{4P}\cosh\left(2PZ\right)\right]_{Z_1(z)}^{Z_2(z)}; \end{aligned} \quad \text{(A.6)}$$

$$g_3(z) = \left[P\sinh\left(PZ\right)\cos\left(KZ\right) +K\cosh\left(PZ\right)\sin\left(KZ\right)\right]_{Z_1(z)}^{Z_2(z)}/\left(P^2+K^2\right);$$

$$g_4(z) = \left[P\cosh\left(PZ\right)\cos\left(KZ\right) +K\sinh\left(PZ\right)\sin\left(KZ\right)\right]_{Z_1(z)}^{Z_2(z)}/\left(P^2+K^2\right).$$

Now, it is interesting to underline, that in the limit of $z\to L$ all the functions $G_\ell(z)\to 0$ for $\ell = 0,1,4$, while for $\ell = 2,3$ some divergent quantities appear, that can be computed by grouping terms in order to obtain finite contributions, in fact:

$$\lim_{z\to L}\frac{R_e(z)}{\sinh\left(P(Z_2(z)-Z_1(z))\right)} = \frac{\alpha_e-\alpha_h}{2P}\left(P^2+K^2\right)\sinh\left(PZ_0\right)\cos\left(KZ_0\right) \quad \text{(A.7a)}$$

$$\lim_{z\to L}\frac{R_o(z)}{\sinh\left(P(Z_2(z)-Z_1(z))\right)} = \frac{\alpha_e-\alpha_h}{2P}\left(P^2+K^2\right)\cosh\left(PZ_0\right)\cos\left(KZ_0\right) \quad \text{(A.7b)}$$

while, the limit values for:

$$\lim_{z\to L}\frac{M(z)}{\sinh\left(P(Z_2(z)-Z_1(z))\right)} \quad \text{and} \quad \lim_{z\to L}\frac{N(z)}{\sinh\left(P(Z_2(z)-Z_1(z))\right)}$$

are obtained form the following equations:

$$F_e(z\to L) = \cosh\left(PZ_0\right)\cos\left(KZ_0\right) + \frac{K}{P}\sinh\left(PZ_0\right)\sin\left(KZ_0\right) \quad \text{(A.8a)}$$

$$F_o(z\to L) = \sinh\left(PZ_0\right)\cos\left(KZ_0\right) + \frac{K}{P}\cosh\left(PZ_0\right)\sin\left(KZ_0\right) \quad \text{(A.8b)}$$

and the corresponding limit values of the functions:

$$\lim_{z\to L}\frac{g_\ell(z)}{\sinh\left(P(Z_2(z)-Z_1(z))\right)} \qquad \ell = 1,2,3,4,5.$$

$$\lim_{z\to L}\frac{M(z)}{\sinh\left(P(Z_2(z)-Z_1(z))\right)} = F_e(z\to L)\,\frac{\cosh\left(2PZ_o\right)+1}{2P}-\frac{\cosh\left(PZ_o\right)\cos\left(KZ_o\right)}{P} - F_o(z\to L)\,\frac{\sinh\left(2PZ_o\right)}{2P} \quad \text{(A.9a)}$$

$$\lim_{z\to L}\frac{N(z)}{\sinh\left(P(Z_2(z)-Z_1(z))\right)} = F_o(z\to L)\,\frac{\cosh\left(2PZ_o\right)-1}{2P}-\frac{\sinh\left(PZ_o\right)\cos\left(KZ_o\right)}{P} - F_e(z\to L)\,\frac{\sinh\left(2PZ_o\right)}{2P}, \quad \text{(A.9b)}$$

odd solutions can be computed with the same procedure.

Notice, that the first momentum of the exciton Hamiltonian can be computed by two simple $1D$ integrations respect with the relative e–h distance z. Finally, the minimization of the effective Bohr radius a is usually very well defined, while the minimum with respect of the transition layer depth $\delta = 1/\mathrm{P}$ is usually very shallow. Notice, that in the present final equations do not appear the numerically tedious 0/0 terms, due to the limit $z = z_e - z_h \to L$. These terms, as pointed out by Combescot et al. in reference [14], make the numerical accuracy of the minimization not well suited for obtaining sensible values of the transition layer depth.

Appendix B

The electric field in the quantum well are given by the following Lippmann-Schwinger equation (Eq. (28) of the text):

$$E_y(z) = E_y^o(z) - 4\pi\frac{\omega^2}{c^2}\sum_m \int\int g(z,z')\ \chi_m(z',z'')\ E_y(z'')dz'dz'' \quad \text{(B.1)}$$

where $E_y^o(z)$ is the general homogeneous solution.

The electric field in the quantum well is given by the general homogeneous solution plus a particular heterogeneous solution:

$$E_y(z) = A\ e^{ik_z z} + B\ e^{-ik_z z} - 4\pi\frac{\omega^2}{c^2}\sum_m \int_0^L\int_0^L g(z,z')\ \chi_m(z',z'')\ E_y(z'')dz'dz'' \quad \text{(B.2)}$$

and, by substituting the exciton susceptibility, we obtain:

$$E_y(z) = E_y^o(z) - 4\pi\frac{\omega^2}{c^2}\sum_m S_m(\omega)\int_0^L g(z,z')\ \Psi_m^*(z')\ dz' \times \int_0^L \Psi_m(z'')\ E_y(z'')dz'' \quad \text{(B.3)}$$

where,

$$S_m(\omega) = \frac{S_o(\omega)}{E_m(\vec{K}_\parallel) - \hbar\omega - i0^+}.$$

Now, applying the operator $\int_0^L dz\ \Psi_{m'}(z)$, we obtain the system:

$$\sum_m [\delta_{m',m} + M_{m'\,m}(\omega)]\ I_m(\omega) = I^o_{m'}(\omega) = A\ \varphi_{m'}(k_z) + B\ \varphi_{m'}(-k_z) \quad \text{(B.4)}$$

where $\varphi_{m'}(k_z) = \int_0^L e^{ik_z z}\ \Psi_{m'}(z)dz$, and the unknown integrate quantities are:
$I_m(\omega) = \int_0^L \Psi_m(z)\ E_y(z)dz$, while the polaritonic matrix elements are:

$$M_{m'm}(\omega) = \frac{\omega^2}{c^2}\ S_o(\omega)\int_0^L\int_0^L \Psi_{m'}(z)\ g(z,z')\ \Psi^*_m(z')\ dz'dz \times \left[E_m(\vec{K}_\parallel) - \hbar\omega - i0^+\right]^{-1} \quad \text{(B.5)}$$

and the solution of the system is:

$$I_m(\omega) = \sum_{m'}\left[\left(\overleftrightarrow{I} + \overleftrightarrow{M}(\omega)\right)^{-1}\right]_{mm'} \times [A\ \varphi_{m'}(k_z) + B\ \varphi_{m'}(-k_z)]. \quad \text{(B.6)}$$

Finally, by substituting this result into the electric field of equation (B2), we obtain:

$$\begin{aligned} E_y(z) =& A\left\{e^{ik_z z} - 4\pi\frac{\omega^2}{c^2}\sum_m S_m(\omega)\ G_m(z) \times \sum_{m'}\left[\left(\overleftrightarrow{I} + \overleftrightarrow{M}(\omega)\right)^{-1}\right]_{m\,m'}\varphi_{m'}(k_z)\right\} \\ &+ B\left\{e^{-ik_z z} - 4\pi\frac{\omega^2}{c^2}\sum_m S_m(\omega)\ G_m(z) \times \sum_{m'}\left[\left(\overleftrightarrow{I} + \overleftrightarrow{M}(\omega)\right)^{-1}\right]_{m\,m'}\varphi_{m'}(-k_z)\right\} \end{aligned} \quad \text{(B.7)}$$

where: $G_m(z) = \int_0^L g(z,z')\ \Psi^*_m(z')\ \ dz'$, and $g(z,z') = \frac{1}{2ik_z}\ e^{ik_z|z-z'|}$.

Appendix C

The dispersion curves of the superlattice system can be computed from equation (34) of the text. The even exciton envelope function for $\vec{r} = 0$ is real for Z-values : $-L/2 < Z < L/2$ (see Eq. (21) of the text),

$$\Psi_m(\vec{r} = 0, Z) = \frac{N_m}{\sqrt{\pi a^3}}\left\{\cos(k_m Z) - \cosh(PZ)\,\frac{\cos(k_m L/2)}{\cosh(PL/2)}\right\}$$

where k_m is the eigenvalues of equation (11) of the text. Its Fourier transform is given by simple algebra,

$$\varphi_m(k_z) = \int_0^L \Psi_m(\vec{r}=0,Z)\ e^{ik_zZ} = \frac{N_m}{\sqrt{\pi a^3}}\left\{e^{ik_zZ}\left[A(Z)+ik_zB(Z)\right]\right\}_{Z=-L/2}^{Z=L/2} \tag{C.1}$$

where,

$$A_m(Z) = \frac{k_m}{k_m^2-k_z^2}\sin(k_mZ) - \frac{P\ \alpha_m}{k_z^2+P^2}\sinh(PZ)$$

$$B_m(Z) = \frac{1}{k_m^2-k_z^2}\cos(k_mZ) + \frac{\alpha_m}{k_z^2+P^2}\cosh(PZ)$$

$$\alpha_m = \cos(k_mL/2)/\cosh(PL/2)$$

and,

$$\varphi_m(k_z) = e^{ik_zL}\frac{2N_m}{\sqrt{\pi a^3}}\left\{\left[A_m(L/2)\ \cos(k_zL/2) - k_zB_m(L/2)\sin(k_zL/2)\right]\right\} = e^{ik_zL}\ \tilde{\varphi}_m(k_z) \tag{C.2}$$

the phase factor takes into account the translation of $L/2$, while the transformed function $\tilde{\varphi}_m$ is a real quantity.

The polaritonic matrix element of equation (B5) is:

$$M_{m',m}(\omega) = \frac{\omega^2}{c^2}S_m(\omega)\int_0^L dZ\,\Psi_{m'}(\vec{r}=0,Z) \times\left\{e^{ik_zZ}\int_0^Z e^{-ik_zZ'}\ \Psi_m^*(\vec{r}=0,Z')\ dZ' + e^{-ik_zZ}\int_Z^L e^{ik_zZ'}\ \Psi_m^*(\vec{r}=0,Z')\ dZ'\right\} S_m(\omega) = \frac{\omega^2}{c^2}S_m(\omega)\left[M^{>}_{m,m'}+M^{<}_{m,m'}\right]$$

and, since:

$$\varphi_{m'}(-k_z)\ \varphi_m^*(-k_z) = \tilde{\varphi}_{m'}(-k_z)\ \tilde{\varphi}_m(k_z) = \left[M^{>}_{m'\,m}(\omega)\right]^* + M^{<}_{m'\,m}(\omega)$$

we obtain the polariton matrix in the final form:

$$M_{m'\,m}(\omega) = \frac{\omega^2}{c^2}\left\{\tilde{\varphi}_{m'}(-k_z)\ \tilde{\varphi}_m(k_z) + 2i\ \mathrm{Im}\left[M^{>}_{m'\,m}\right]\right\}S_m(\omega) \tag{C.3}$$

where real and imaginary part are separated.

Now, by some simple algebra, we obtain:

$$\begin{aligned}\mathrm{Im}\left[M^{>}_{m',m}(\omega)\right] = \frac{2N_mN_{m'}}{\pi a^3}\{&[A_m(L/2)\sin(k_zL/2) + k_zB_m(L/2)\cos(k_zL/2)]\,[A_m(L/2)\cos(k_zL/2) - k_zB_m(L/2)\sin(k_zL/2)] - k_z\left[\frac{1}{2\,(k_m^2-k_z^2)}\right.\\ &\times\left(\frac{\sin((k_{m'}-k_m)L/2)}{k_{m'}-k_m}+\frac{\sin((k_{m'}+k_m)L/2)}{k_{m'}+k_m}\right)\\ &+\frac{\alpha_m}{(P^2+k_z^2)\,(P^2+k_{m'}^2)}\,(P\sinh(PL/2)\cos(k_{m'}L/2)\\ &+k_{m'}\cosh(PL/2)\sin(k_{m'}L/2)) - \frac{\alpha_{m'}}{(k_m^2-k_z^2)\,(P^2+k_m^2)}\\ &\times(P\sinh(PL/2)\cos(k_mL/2)+k_m\cosh(PL/2)\\ &\left.\times\sin(k_mL/2)) - \frac{\alpha_m\alpha_{m'}}{4\,(P^2+k_z^2)}\,(L+\sinh(PL))\right]\Big\}\end{aligned} \tag{C.4}$$

while the product of the Fourier transform is,

$$\begin{aligned}\varphi_{m'}(-k_z)\ \varphi_m^*(-k_z) = &\frac{4N_mN_{m'}}{\pi a^3}\\ &\times\{[A_{m'}(L/2)\cos(k_zL/2) - k_zB_{m'}(L/2)\sin(k_zL/2)]\\ &\times[A_m(L/2)\cos(k_zL/2) - k_zB_m(L/2)\sin(k_zL/2)]\}.\end{aligned} \tag{C.5}$$

Notice, that the polaritonic matrix is a product of the self-energy,

$$\Sigma_{m'm}(\omega) = \frac{\omega^2}{c^2}\ S_o(\omega)\int_0^L\int_0^L \Psi_{m'}(z)\ g(z,z')\ \Psi_m^*(z')\ dz'dz \tag{C.6}$$

plus a diagonal matrix of the energy denominators,

$$S_{m\,m'} = \left[E_m(\vec{K}_\parallel) - \hbar\omega - i0^+\right]^{-1}\delta_{m,m'}.$$

Now, let us consider the inverted matrix:

$$\left[\left(\overleftrightarrow{I}+\overleftrightarrow{M}(\omega)\right)^{-1}\right]_{m\,m'} = S_{m\,m}(\omega)\ \left[\left(\overleftrightarrow{S^{-1}}(\omega) + \overleftrightarrow{\Sigma}(\omega)\right)^{-1}\right]_{m\,m'} = S_{m\,m}(\omega)\ P_{m\,m'}(\omega)$$

and, the polariton matrix is:

$$P_{m'\,m}(\omega) = \left[E_{m'}(K_\parallel) - \hbar\omega - i\Gamma_{NR}\right]\delta_{m'\,m} + \Sigma_{m'\,m}(\omega) \tag{C.7}$$

where the self-energy matrix is:

$$\Sigma_{m'\,m}(\omega) = \Sigma'_{m'\,m}(\omega) + i\Sigma''_{m'\,m}(\omega) = \frac{\omega^2}{c^2}\frac{S_o(\omega)}{2k_z}\left\{\mathrm{Im}\left[M^{>}_{m',m}\right] - i\,\tilde{\varphi}_{m'}(-k_z)\ \tilde{\varphi}_m(k_z)\right\}. \tag{C.8}$$

Finally,

$$\Delta_{\pm\mp}(\omega) = -\frac{\omega^2}{c^2}\frac{S_o(\omega)}{2k_z}e^{\pm ik_z L/2 \mp ik_z L/2} \times \sum_{m\,m'} \tilde{\varphi}_m(\pm k_z) \left(\overleftrightarrow{P^{-1}}\right)_{m\,m'} \tilde{\varphi}_{m'}(\mp k_z). \quad \text{(C.9)}$$

Therefore, the optical response of a single quantum well and the dispersion curves of $\lambda/2$ Bragg system can be computed by equations (31) and (34) respectively of the text.

References

1. T. Ikawa, K. Cho, Phys. Rev. B **66**, 085338-1 (2002)
2. K. Cho, T. Ikawa, Phys. Stat. Sol. (a) **190**, 401 (2002)
3. L. Pilozzi, A. D'Andrea, K. Cho, Phys. Rev. B **69**, 205311 (2004)
4. E. Yablonovich, Phys. Rev. Lett. **58**, 2059 (1987)
5. E.L. Ivchenko, A.I. Nesvizhskii, S. Jorda, Phys. Sol. St. **36**, 1156 (1994)
6. T. Stroucken, A. Knorr, P. Thomas, S.W. Koch, Phys. Rev. B **53**, 2026 (1995)
7. M. Hubner, J. Kuhl, T. Stroucken, A. Knorr, S.W. Koch, R. Hey, K. Ploog, Sol. St. Com. **105**, 105 (1998)
8. L.C. Andreani, G. Panzarini, A.V. Kavokin, M.R. Vladimirova, Phys. Rev. B **57**, 4670 (1998)
9. M. Hubner, J.P. Prineas, C. Ell, P. Brick, E.S. Lee, G. Khitrova, H.M. Gibbs, S.W. Koch, Phys. Rev. Lett. **76**, 4199 (1999)
10. G.R. Hayes, J.L. Staehli, U. Oesterle, B. Deveaud, R.T. Phillips, C. Ciuti, Phys. Rev. Lett. **83**, 2837 (1999)
11. S. Nojima, Phys. Rev. B **59**, 5662 (1999)
12. Lev I. Deych, A. Yamilov, A.A. Lisyansky, Opt. Lett. **23**, 1705 (2000)
13. E.L. Ivchenko, M.M. Voronov, M.V. Erementchouk, L.I. Deych, A.A. Lisyansky, Phys. Rev. B. **70**, 195106 (2004)
14. M. Combescot, R. Combescot, B. Roulet, Eur. Phys. J. **22**, 89 (2001); M. Combescot, R. Combescot, B. Roulet, Eur. Phys. J. B **23**, 139 (2001)
15. A. D'Andrea, R. Del Sole, Phys. Rev. B **41**, 1413 (1990)
16. *Spatial dispersion in solids and plasmas*, edited by. P. Halevi, Vol. 1 (North-Holland, 1992), p. 392
17. A. D'Andrea, N. Tomassini, Phys. Rev. B **47**, 7176 (1993) 430-4
18. D. Greco, R. Cingolati, A. D'Andrea, N. Tomassini, L. Vanzetti, A. Franciosi, Phys. Rev. B **54**, 16998 (1996)
19. R. Atanasov, F. Bassani, A. D'Andrea, N. Tomassini, Phys. Rev. B **50**(19), 14381 (1994)
20. A. D'Andrea, D. Schiumarini, L. Pilozzi, N. Tomassini, in preparation
21. In reference [14], the authors claim that the exciton model of reference [15], give a wrong exciton behaviour at quantum well interfaces, because in strong disagreement with the heuristic "hard sphere model" and with their "exact" results